Meteorologische Zeitschrift, Vol. 23, No. 5, 467–481 (published online September 26, 2014)

Deviations from a general nonlinear wind balance: Local and zonal-mean perspectives

Almut Gassmann*

Leibniz-Institut für Atmosphärenphysik, Kühlungsborn, Germany

(Manuscript received December 17, 2013; in revised form July 14, 2014; accepted July 14, 2014)

Abstract

The paper introduces the active wind as the deviation from a general local wind balance, the inactive wind. The inactive wind is directed along intersection lines of Bernoulli function and potential temperature surfaces. In climatological steady state, the inactive mass flux cannot participate in net-mass fluxes, because the mean position of the mentioned intersection lines does not change. A conceptual proximity of the zonal-mean active wind to the residual wind as occurring in the transformed Eulerian mean equations suggests itself. The zonal- and time-mean active wind is compared to the residual wind for the Held-Suarez test case. Similarities occur for the meridional components in the zone of Rossby wave breaking in the upper troposphere equatorward of the jet. The vertical components are similar, too. However, the vertical active wind is much stronger in the baroclinic zone. This is due to the missing vertical eddy flux of Ertel's potential vorticity (EPV) in the TEM equations. The largest differences are to be found in the boundary layer, where the active wind exhibits typical pattern of Ekman dynamics. Instantaneous active wind vectors demonstrate mass-inflow for lows and mass-outflow for highs in the boundary layer. An active meridional wind is associated with a filamentation of EPV in the zone of Rossby wave breaking in about 300 hPa. Strong gradients of EPV act as a transport barrier.

Keywords: nonlinear wind balance, dynamic state index (DSI), TEM equations

1 Introduction

The investigation of wave-induced mean flow covers two aspects. First, the divergence of the Eliassen-Palm flux is interpreted as a wave-induced force for the mean zonal momentum equation. Second, the associated driving of a residual circulation as a consequence of the wave-forcing is interpreted as the actual zonally averaged mass circulation in the meridional plane. It is used to explain the Brewer-Dobson circulation in the stratosphere. The second point – the physical reality of the residual circulation – resides on the restriction inherent in the first point concerning the Eliassen-Palm flux, namely the assumption of an underlying wave theory for small amplitude waves. If one is interested in the determination of a residual mass circulation, is there a way to circumvent the linear-wave assumption as necessary in the first point? We have to keep in mind that the actual data we use when determining the residual circulation do not inherently contain linear waves. We use data stemming from full nonlinear models of the atmosphere. The main question to answer is: Can we get access to net mass fluxes, or residual flow, without the vehicle of a linear wave theory?

Accepting for a moment linear wave theory. Then, we can investigate idealized linear waves and ask for their contribution to the acceleration of the zonal mean flow. Those idealized waves are supposed to be linear, conservative, and steady. Andrews and McIntyre (1976, 1978) and Boyd (1976) demonstrated that such waves do not accelerate the zonal mean flow. Hence, an associated residual circulation in the meridional plane cannot exist. Therefore, a subsequent step to answer the question how and why a zonal mean residual circulation in the meridional plane may develop was to remove the inherent circulation of the idealized waves from the zonally averaged Eulerian mean flow in the meridional plane $\{v^*, w^*\} = \{\bar{v}, \bar{w}\} - \{\bar{v}^{\mathrm{wave}}, \bar{w}^{\mathrm{wave}}\}$. This step is equivalent to the addition of the Stokes drift $\{v^*, w^*\} = \{\bar{v}, \bar{w}\} + \{v^{\mathrm{St}}, w^{\mathrm{St}}\}$. Such, the circulation inherent in the idealized waves can be translated into a Lagrangian viewpoint. Notional fluid particles follow 'statistically closed' orbits 'in a sense that no large-scale dispersion or Lagrangian-mean advection can occur' (Andrews et al. (1987), Section 9.4.2). Even though those particles undergo a permanent wavy motion, there is no net force that pushes them out of their orbits, neither in meridional nor in vertical direction. Note however, that even though one considers fluid particles in this argumentation, those fluid particles are notional and exist only within the framework based on linear wave theory. One has also to recognize that it is linear wave theory which requires the mass flux of idealized waves to be non-divergent. Then, since the zonal mean total mass flux is also non-divergent in the meridional plane, the residual mass flux is non-divergent, too. All versions of the transformed Eulerian mean (TEM) equations (Andrews and McIntyre; 1976, 1978) postulate that

*Corresponding author: Almut Gaßmann, Leibniz-Institut für Atmosphärenphysik e. V. an der Universität Rostock, Schlossstraße 6, 18225 Kühlungsborn, Germany, e-mail: gassmann@iap-kborn.de

DOI 10.1127/metz/2014/0568

Gebrüder Borntraeger Science Publishers, Stuttgart, www.borntraeger-cramer.com

the zonal mean mass flux induced by idealized waves can be represented by a stream function (Vallis (2006), page 309). Plumb and Ferrari (2005) call this the 'quasi-Stokes stream function'.

The perception of closed wavy orbits is a very natural one. When dropping now the wave-confined viewpoint we retain this orbit idea and ask whether there exists similarly a nonlinear flow field[1] with closed streamlines. Still, this flow field is an idealized one without friction, diabatic heating or cooling, and in steady state. Trajectories and streamlines coincide in this case by definition. Because of the steady state character, we denote its associated wind field as the *inactive* wind field. For arbitrary flows, any deviation from this inactive wind we will call the *active* wind. This deviation is associated with a net mass flux, namely that portion of the mass flux which does not follow the streamlines belonging to the inactive wind. As will be shown later on, such a deviation occurs as a result of unsteady, diabatic, and frictional flow. In contrast to the residual mass flux explained in the context of linear wave theory, this net mass flux is divergent. The regions where its divergence and convergence become obvious are where the mass flux enters or leaves the streamlines belonging to the inactive wind. The associated mass exchange between inactive and active parts of the flow is impossible to be described in the wave-confined view discussed in the previous paragraph, because the residual mass stream function and the stream function of idealized waves are both non-divergent in the meridional plane.

The definition of inactive and active winds relies on the general nonlinear non-hydrostatic compressible equations with the equation of motion in vector-invariant form. This approach is independent of any specific vertical coordinate system. In contrast, linear wave theory has to make use of a specifically chosen coordinate system and the assumption of small amplitude perturbations defined with respect to a mean flow defined in that man-chosen coordinate system.

The paper wants to provide a comparison between the two sketched concepts: (i) the net atmospheric mass fluxes associated with the active wind (flow-confined view), and (ii) the residual mass fluxes associated with the TEM viewpoint (wave-confined view). The flow-confined view provides some new aspects. Zonal and temporal averaging are possible to be performed after the transformation of the equations and the velocities, and not prior to this step as in the TEM framework. Three-dimensional aspects of the net mass fluxes become visible. In the future, it will be possible to compare time averaged net mass fluxes with the three-dimensional TEM residual mass fluxes of Kinoshita et al. (2010). For the practical question concerning how smaller scale gravity waves contribute to net mass fluxes in the atmosphere, it will become possible to investigate the output of regional models which do not have zonally periodic boundary conditions.

[1] Remember the difference between a flow field and a wave field.

As an example we consider here the Held-Suarez experiment (Held and Suarez, 1994). This is the simplest experimental setup to investigate the mean climate. It contains already all features that are essential in our context: dynamical and frictional forcing as well as differential heating. Even though this experiment does not include the stratosphere, residual and active mass fluxes can be studied. Here, this test case is modified by inserting an elliptically shaped mountain range of 1000 m maximum height between 30 ° and 60 ° North and a half width of 1500 km. The so modified test case is run for 1500 days with the ICON-IAP model (Gassmann, 2013). This model discretizes the full non-hydrostatic compressible equations for a shallow atmosphere on a hexagonal C-grid and a height-based terrain-following hybrid vertical coordinate. A horizontal resolution of 120 km and 26 vertical levels are employed for the present study. The time-mean diagnostics skips the first 250 days during which the model is still adapting to the statistically steady state.

The paper is structured as follows: Section 2 introduces the flow confined viewpoint with a thorough motivation of inactive and active winds. Section 3 compares the flow-confined and the wave-confined views of the net mass fluxes in the meridional plane for the Held-Suarez test. Section 4 concludes the paper.

2 Flow-confined viewpoint

2.1 The inactive wind

The prognostic velocity equation with the nonlinear advection term in its vector-invariant form reads

$$\partial_t \mathbf{v} = -\boldsymbol{\omega}_a \times \mathbf{v} - \nabla B + c_p \Pi \nabla\theta + \mathbf{F}_r. \qquad (2.1)$$

Here, $\boldsymbol{\omega}_a$ is the absolute vorticity vector, $B = \mathbf{v}^2/2 + c_p\Pi\theta + \Phi$ the Bernoulli function, Π the Exner pressure, θ the potential temperature, Φ the geopotential, and $\mathbf{F}_r$ is a frictional force. If we consider moist atmospheric flow, θ represents the virtual potential temperature. Next, we apply the $\nabla\theta\times$ operation, use the vector identity $\nabla\theta \times (\boldsymbol{\omega}_a \times \mathbf{v}) = \boldsymbol{\omega}_a(\mathbf{v}\cdot\nabla\theta) - \mathbf{v}(\nabla\theta\cdot\boldsymbol{\omega}_a)$, rearrange, and obtain

$$\nabla\theta\times(\partial_t\mathbf{v}-\mathbf{F}_r)+\boldsymbol{\omega}_a(\mathbf{v}\cdot\nabla\theta) = \mathbf{v}(\nabla\theta\cdot\boldsymbol{\omega}_a)-\nabla\theta\times\nabla B. \quad (2.2)$$

The last term on the left hand side can be replaced by employing the prognostic equation for the potential temperature

$$\partial_t\theta + \mathbf{v}\cdot\nabla\theta = Q, \qquad (2.3)$$

where Q is the diabatic heating. The first term on the right hand side of (2.2) can be written in a more convenient form if we use the definition of EPV (Ertel's potential vorticity), $P := \nabla\theta\cdot\boldsymbol{\omega}_a/\varrho$. Then we obtain

$$\nabla\theta\times(\partial_t\mathbf{v}-\mathbf{F}_r) - \boldsymbol{\omega}_a(\partial_t\theta - Q) = \varrho\mathbf{v}P - \nabla\theta\times\nabla B. \quad (2.4)$$

Note that this derivation has already been reported by Schär (1993), and the result (2.4) is identical to equation (18) of Schär (1993). The interpretation of the total flux of EPV

$$\mathbf{J} = \nabla\theta \times \mathbf{F}_r - \omega_a Q + \varrho \mathbf{v} P - \nabla\theta \times \nabla B \tag{2.5}$$

is ambiguous in the literature as discussed by Davies-Jones (2003). Whereas most authors (Schär (1993), Haynes and McIntyre (1987, 1990)) exclude $\nabla\theta \times \nabla B$ from the total EPV-flux because it is irrelevant when its divergence is taken in the prognostic EPV-equation, we retain this term in the present consideration. The reason for retaining it lies in the observation that for steady ($\partial_t \cdot = 0$), frictionless ($\mathbf{F}_r = 0$), and adiabatic ($Q = 0$) flows the advective EPV-flux is balanced by (cf. Schär (1993) equation (6))

$$\varrho \mathbf{v} P = \nabla\theta \times \nabla B. \tag{2.6}$$

The goal is here to retain an information about this balance in the total EPV-flux. The associated wind field is

$$\mathbf{v} = \frac{\nabla\theta \times \nabla B}{\varrho P}. \tag{2.7}$$

As pointed out by Lange (2002), (2.7) is the most general balanced wind relation that can be found. As it involves both, the momentum equation and the thermodynamic equation, it is a steady state 3D vector balance of all non-frictional forces under the constraint of adiabatism, hence a balance of forces on an isentropic surface. Like the geostrophic wind, (2.7) becomes undefined if the denominator vanishes. All known geostrophic wind forms of appearance are approximations to that general form and describe a linear balance of only the Coriolis force and the pressure gradient force. Two features distinguish the wind (2.7) from the geostrophic wind. First, the geostrophic balance disregards inertial forces, which make up the relative vorticity and the kinetic energy in (2.7). Therefore the wind (2.7) expresses a nonlinear balance. Second, the geostrophic balance considers only hydrodynamic aspects, but not thermodynamic aspects of the flow. The thermodynamic aspect as the constraint of adiabatism is involved in (2.7) via the $\nabla\theta\times$ operation. The comparable $\mathbf{k}\times$ operation in case of the geostrophic wind is however motivated by the fact that the Coriolis force acts exclusively horizontally. The $\mathbf{k}\times$ operation is unrelated to any thermodynamic argumentation.

At this point we define the *inactive* wind as

$$\mathbf{v}_{ia} := \frac{\nabla\theta \times \nabla B}{\varrho P}. \tag{2.8}$$

The velocity $\mathbf{v}_{ia}$ is directed along the intersection lines of θ and B surfaces (Schär, 1993). We chose the denotation *inactive* because of two reasons. First, the advective EPV-flux divergence associated with the inactive wind vanishes upon taking the divergence and is thus a 'do-nothing flux' in the EPV equation (Haynes and McIntyre, 1990). Second, processes that convert kinetic energy into internal or potential energy and vice versa are associated with the terms $\varrho\mathbf{v}\cdot\nabla B$ and $c_p\Pi\varrho\mathbf{v}\cdot\nabla\theta$, as can be inferred when scalar multiplying (2.1) with $\varrho\mathbf{v}$. Obviously, since $\mathbf{v}_{ia}$ is perpendicular to both, ∇B and $\nabla\theta$, the inactive wind is not associated with energy conversions. The generalized Coriolis term does not perform work by definition, because $\varrho\mathbf{v}\cdot(\boldsymbol{\omega}_a\times\mathbf{v}) = 0$. Hence, the inactive wind is neither involved in the evolution of EPV nor in the evolution of the single forms of energy at a certain place in the atmosphere. Even though the geostrophic wind is closely related to the inactive wind, the geostrophic wind is not inactive since it may cross isentropic surfaces.

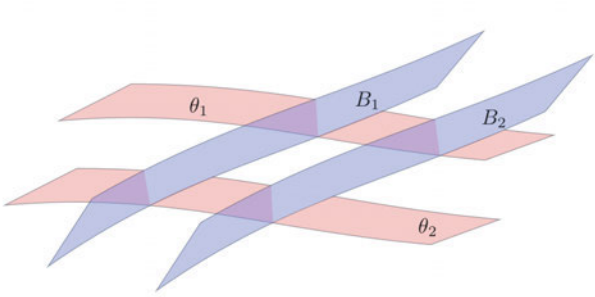

Figure 1: A tube surrounded by two adjacent θ- and two adjacent B-surfaces.

For actually encountered inactive flow, particles are trapped in vector tubes $\nabla\theta\times\nabla B$. One tube is surrounded by two adjacent θ- and two adjacent B-surfaces (Fig. 1). Every tube is closed in the atmosphere unless at least one of the involved boundary surfaces intersects the ground[2]. As the particles are trapped in the tubes, a net mass transport that leaves or enters the tubes in any direction does not take place. Trajectories and streamlines coincide for actually encountered inactive flow because this flow is steady.

The inactive flow can be considerably meandering. Under the wave-viewpoint we would say that it contains eddies with respect to a zonal mean. The meandering of an actual flow is shown in Fig. 2. In Fig. 2(a), a selected B-isoline with a value of 314000 J/kg is plotted together with geometric height (in colors) on the 315 K isentropic surface. As the data from the ICON-IAP model are not available on isentropes, arbitrary data of the IFS model are taken for this illustration. Two issues are important here. First, the horizontal wind vectors are almost parallel to the selected B-isoline. That signifies the predominance of the inactive wind within the actual wind. Deviations of the actual wind from the inactive wind are comparably small. Second, when following one B-isoline the lowermost point is mostly found further poleward than

[2]If a tube intersects the ground the flow cannot considered inactive any longer because of frictional effects. For thought experiments with the inactive wind we exclude the intersection of tubes with the surface.

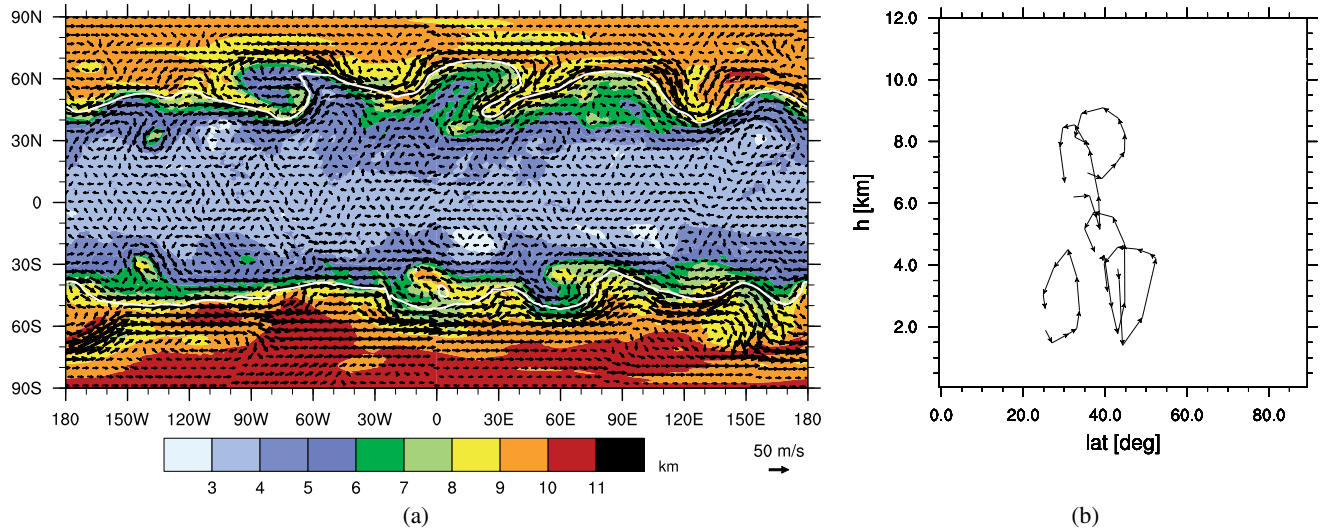

Figure 2: Illustration of meandering flow. a) the horizontal wind (arrows) is almost parallel to the white B-isoline (here 314000 J/kg) on an isentrope (here 315 K). The geometric height of the isentrope is color-shaded. For that illustration, IFS model output data are taken for an arbitrary date in October 2011. b) longitudinally consecutive intersection points ($\Delta\lambda = 6.25\,°$) of 5 arbitrarily selected $\{\theta, B\}$-pairs are connected by arrows. For that illustration, ICON-IAP model output data are taken from an arbitrary time step of the Held-Suarez test.

the uppermost point. Fig. 2(b) shows a side view of the meandering of the actual flow for an arbitrary timestep of the Held-Suarez test run with the ICON-IAP model. Here, intersection points of some selected θ and B isolines for consecutive longitudes are connected by arrows. Such a sequence of arrows represents B-isolines in the same way as the white contour lines in Fig. 2(a). If the flow was indeed inactive, such arrows would illustrate particle orbits. As known from theory (Andrews et al. (1987), Section 4.5.3 or Holton (2004), Fig. 12.5) idealized orbits are helical for stationary Rossby waves. Their projections onto the meridional plane yield slanted ellipses. Indeed, two of the three upper streamlines in Fig. 2(b) resemble slanted ellipses, where the lowermost points are further poleward than the uppermost points, just like mentioned for the B-isolines in Fig. 2(a).

2.2 Deviations from the inactive wind: the active wind

We are interested in the atmospheric flow part which is not inactive, but active. The actual wind will usually deviate from the inactive wind. Therefore we define the *active* wind as

$$\mathbf{v}_a := \mathbf{v} - \mathbf{v}_{ia} = \mathbf{v} - \frac{\nabla\theta \times \nabla B}{\varrho P}. \tag{2.9}$$

It has to be noted that $\mathbf{v}_{ia}$ depends on $\mathbf{v}$ because the kinetic energy as a part of the Bernoulli function and the vorticity vector as a part of EPV are functions of $\mathbf{v}$. Hence it is essential to qualify equation (2.8) as a *definition* (and not a *balance* like (2.7)) of the inactive part of the wind.

An dynamically active part of the EPV-flux can be defined as

$$\varrho \mathbf{v}_a P := \varrho \mathbf{v} P - \nabla\theta \times \nabla B. \tag{2.10}$$

The EPV-flux (2.10) is associated with diabatic heating, frictional forcing, and transient disturbances, because from (2.4) we see

$$\begin{aligned} &\nabla\theta \times (\partial_t \mathbf{v} - \mathbf{F}_r) - \omega_a(\partial_t\theta - Q) \\ &= \varrho \mathbf{v}_a P = -\nabla\theta \times (\boldsymbol{\omega}_a \times \mathbf{v}_a) + \omega_a(\mathbf{v}_a \cdot \nabla\theta). \end{aligned} \tag{2.11}$$

We observe that the second terms on both sides of (2.11) establish together the potential temperature equation multiplied with the absolute vorticity

$$\omega_a \partial_t \theta = \omega_a(-\mathbf{v}_a \cdot \nabla\theta + Q), \tag{2.12}$$

because $\mathbf{v}_{ia} \cdot \nabla\theta = 0$. Substraction of (2.12) from (2.11) gives a modified momentum equation projected onto isentropes

$$\nabla\theta \times \partial_t \mathbf{v} = \nabla\theta \times (-\boldsymbol{\omega}_a \times \mathbf{v}_a + \mathbf{F}_r). \tag{2.13}$$

It is known that a disturbance-induced (mean) 'force' corresponds to an EPV-flux (McIntyre and Norton, 1990). Here we see that the EPV-flux influences both, the thermodynamic part $\partial_t\theta$ and the hydrodynamic part $\partial_t \mathbf{v}$ of the flow. Only if one considers the momentum equation on an isentropic surface for adiabatic flow ($Q = 0$), the correspondence between EPV-flux and disturbance-induced force is justified. It seems that $-\boldsymbol{\omega}_a \times \mathbf{v}_a$ in the transformed momentum equation (2.13) is a fictitious force like the Coriolis force, but it is in fact a substitution for a net significant real force. The transformed equations (2.12) and (2.13) are meaningful as long as the stratification $\nabla\theta$ and the absolute vorticity $\boldsymbol{\omega}_a$ are significant. This corresponds to the requirement that the EPV has a significant value.

The equations (2.12) and (2.13) both use the transformed velocity $\mathbf{v}_a$. Therefore they resemble the TEM equations. In contrast to the TEM equations, no assumption about waves or means and no zonal or temporal

averaging was involved during the transformation step. The TEM equations for β-plane geometry as given in Andrews et al. (1987) read

$$\partial_t \overline{u} - f_0 v^* = \varrho_r^{-1} \nabla \cdot \mathbf{F} - X \tag{2.14}$$

$$\partial_t \overline{\theta} + w^* \partial_z \overline{\theta} = \overline{Q} \tag{2.15}$$

$$\partial_y v^* + \varrho_r^{-1} \partial_z (\varrho_r w^*) = 0 \tag{2.16}$$

$$f_0 \partial_z \overline{u} + H^{-1} Re^{-\kappa z/H} \partial_y \overline{\theta} = 0. \tag{2.17}$$

Here

$$v^* = \overline{v} - \varrho_r^{-1} \partial_z \psi = \overline{v} - \overline{v}^{\text{wave}} = \overline{v} + \overline{v}^{\text{St}} \tag{2.18}$$

$$w^* = \overline{w} + \varrho_r^{-1} \partial_y \psi = \overline{w} - \overline{w}^{\text{wave}} = \overline{w} + \overline{w}^{\text{St}} \tag{2.19}$$

are also transformed, namely residual, meridional and vertical velocities. The transformation relies on substracting the mass stream function $\psi = \varrho_r \overline{v'\theta'}/\overline{\partial_z \theta}$ of idealized waves from the total zonal mean mass stream function. Such waves have no effect on the mean flow and are thus removed in order to extract the effect of transient and dissipating waves. The TEM equations impose a non-divergent continuity equation for the residual mass fluxes. They constrain the meridional velocity equation to reduce to the geostrophic balance. In turn, this implies the thermal wind balance for the zonal-mean zonal wind. The zonal-mean eddy forcing is described by the divergence of the Eliassen-Palm flux $\mathbf{F}$. X is a zonal-mean frictional force and H is the scale height.

2.3 Interpretation of inactive and active flow

The splitting of the total wind into an inactive and an active part raises the transition from one portion to the other an essential feature of net atmospheric mass fluxes. This can be understood in the following way. Consider the continuity equation

$$\begin{aligned} \partial_t \varrho &= -\nabla \cdot (\varrho \mathbf{v}_{ia}) - \nabla \cdot (\varrho \mathbf{v}_a) \\ &= \frac{\varrho \mathbf{v}_{ia}}{P^2} \cdot \nabla \frac{P^2}{2} - \nabla \cdot (\varrho \mathbf{v}_a). \end{aligned} \tag{2.20}$$

The divergence of the inactive mass flux does only vanish for actually encountered inactive flow. Bernoulli function and EPV streamlines coincide in this case. This was a motivation for Weber and Névir (2008) and Claussnitzer et al. (2008) to diagnose extreme weather events via the deviation from this energy-vorticity equilibrium state. As a self-evident diagnostic these authors defined the dynamic state index (DSI)

$$\text{DSI} := \frac{1}{\varrho} \frac{\partial(P, \theta, B)}{\partial(x, y, z)}. \tag{2.21}$$

This index can be reformulated such as to be expressed as a negative enstrophy advection with the inactive wind

$$\text{DSI} = \mathbf{v}_{ia} \cdot \nabla \frac{P^2}{2}. \tag{2.22}$$

The DSI displays a typical dipole structure where negative values occur at the front side of an approaching low pressure system and positive values occur at the back (Weber and Névir, 2008; Claussnitzer et al., 2008). Fig. 3 displays a weighted DSI,

$$\text{DSI}^* := \varrho \text{DSI}/P^2 = -\nabla \cdot (\varrho \mathbf{v}_{ia}), \tag{2.23}$$

together with the active wind vectors for an arbitrary time step of the Held-Suarez test on a model level in the boundary layer. The negative and positive DSI* values are associated with divergences and convergences of inactive mass fluxes. As can be deduced from (2.20), the DSI* is a source term with respect to the mass associated with the active part of the flow

$$\partial_t \varrho + \nabla \cdot (\varrho \mathbf{v}_a) = \text{DSI}^*. \tag{2.24}$$

The vectors displayed in Fig. 3 make visible that the weighted DSI* acts predominantly like a source term for the active mass flux divergence. The figure also indicates that it is the active part of the wind which transports mass from high pressure to low pressure systems in the boundary layer. If any boundary of a tube $\nabla\theta \times \nabla B$ intersects the surface, the inactive mass flux must detrain from the tube and become interpreted as an active mass flux. Together with the physical no-slip boundary condition for viscous flow, $\mathbf{v}_{\text{surf}} = 0$, we find $\mathbf{v}_{ia,\text{surf}} = -\mathbf{v}_{a,\text{surf}}$. Hence, the active wind does not vanish at the surface. We could also state that even if the air does physically not move at the surface, it is moved out of the corresponding tube because of surface friction.

Another example of a $\mathbf{v}_a$-field is shown in Fig. 4. Here, the horizontal active wind is plotted on a model level of about 300 hPa together with the weighted DSI* (upper panel), Ertel's potential vorticity (middle panel), and wind speed (lower panel). Again it is obvious that a positive DSI* (upper panel) is a source for the active wind and its negative value is a sink. The structure of the EPV field (middle panel) can be interpreted to first order as the structure of the absolute vorticity field. The magnitude of $\mathbf{v}_a$ is the larger the smaller (larger) the absolute vorticity on the northern (southern) hemisphere. This is because the acceleration of the wind depends on both, the absolute vorticity and the active wind (see equation (2.13)). To achieve a comparable acceleration, the active wind must be larger in magnitude where the absolute vorticity is smaller in magnitude and vice versa. The mostly westward pointing active wind vectors are an indicator for the eastward displacement of the whole wave structure. This can be explained by consideration of the wind speed field (lower panel). On the northern hemisphere, westward pointing active wind vectors indicate a northward acceleration of the local wind. This means an increase of the wind speed towards the north if the jet is approaching with its northward pointing flank and a decrease of the southward wind if the southward pointing flank is leaving. The such indicated eastward movement is not associated with a net meridional active wind. In the main jet region, the active meridional wind

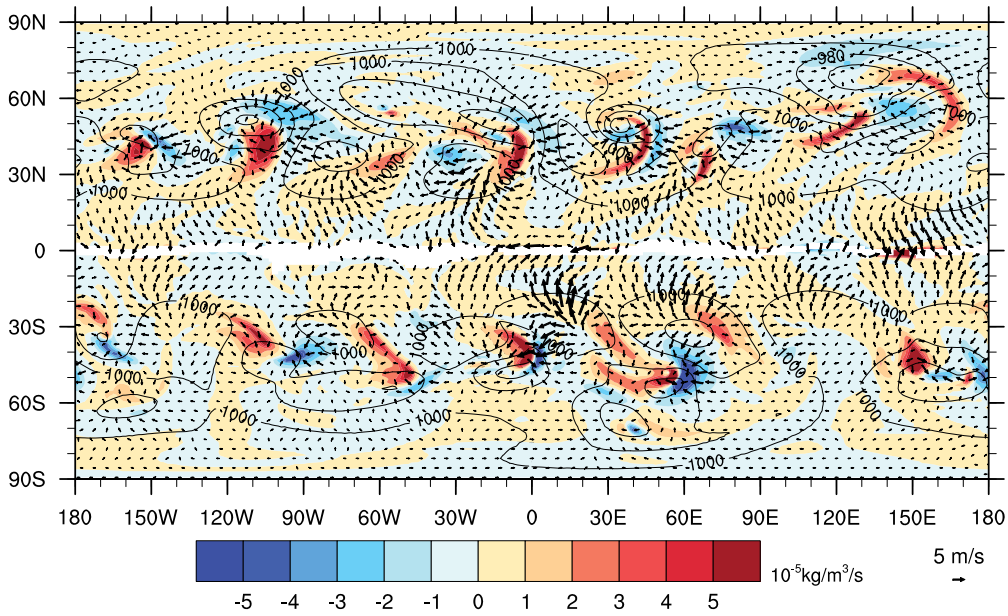

Figure 3: DSI* (colors), sea level pressure (contours, hPa), and active horizontal wind vectors in about 200 m height, the second lowest model level. Data are set undefined in the area near the equator where the EPV becomes insignificant.

may have positive and negative components. However, further equatorward in the surf zone, the EPV values (middle panel) are stripped out in filaments. Here it is more often the case that active wind vectors tend to point poleward. This indicates a net poleward mass transport due to dissipating Rossby waves. The middle panel of Fig. 4 also demonstrates that a steep gradient in EPV is a barrier for the active mass flux. This is a well-known phenomenon and important for the dynamics associated with the formation of the Antarctic ozone hole. Meridional active wind components occur where the gradients of EPV are weak.

The active wind possesses a close similarity to the ageostrophic wind, because it is likewise the deviation of the actual wind from a dominating wind balance. Therefore one expects to see similar behavior of the active wind as for the ageostrophic wind in Figs. 3 and 4. For the boundary layer part in Fig. 3 the active wind arrows indicate the Ekman layer circulation like it is known from the ageostrophic wind component in the boundary layer. For the jet region in Fig. 4 one expects to see the typical divergence and convergence pattern in the jet entrance and exit regions as known from the ageostrophic wind. This is indeed partly true. High DSI* values are associated with divergent active wind regions and low DSI* values signify convergent active wind regions. On the northern hemisphere, jet exit regions in Fig. 4 feature high DSI*-values left to the low DSI*-values on the right, jet entrance regions are characterized by high values to the right and low values to the left. These pattern are as expected from the ageostrophic wind characteristics. However, all those pattern are to be found south of the main jet and are not centered with respect to the jet core. This is can be traced to the fact that the geostrophic wind is defined with the Earth vorticity f in the denominator, but the inactive wind uses the absolute vorticity at this place. As already discussed, the active wind is smaller in magnitude where the absolute vorticity is larger in magnitude and vice versa. Hence, also the divergence/convergence pattern can not be centered with respect to the jet core.

A local crossing of the tube's boundaries – which means a non-vanishing $\mathbf{v}_a$ – might indicate two processes. Either, the tube itself is advected, or particles indeed cross the boundaries of the tube irreversibly. The advective character is exemplified in Fig. 5 (upper panel). Here, a vertical cross section of the active vertical wind is plotted together with the isentropes in about 45 ° North. Positive (negative) w_a-values occur where the θ-isoline bends downward (upward) indicating an adiabatic lifting (sinking). Such, the whole wave structure is advected eastward. For comparison, the mentioned correlation is not found for the actual vertical wind (Fig. 5, lower panel). Since the θ, B-tubes are closed in the atmosphere and do not have a drift in a mean climate, we expect that a simple advection as discussed for θ in Fig. 5 (upper panel) would not leave a net mass flux. The dominating blue colors in Fig. 5 (upper panel), however, lead to the conjecture that a time and zonal mean would leave a net downward mass flux. Hence, if it turns out after averaging that we see a negative w_a, then mainly downward motion associated with diabatic cooling and crossing of θ-surfaces must have left its traces. Concerning the traces left by wave-breaking associated with the crossing of the B-isolines, we consider non-linear energy cascades associated with such a process. Waves convert kinetic energy into available energy and vice versa. The conversion $-\mathbf{v}_a \cdot \nabla B + c_p \Pi \varrho \mathbf{v}_a \cdot \nabla \theta$ is always significant, whereas – as already discussed – the inactive wind can-

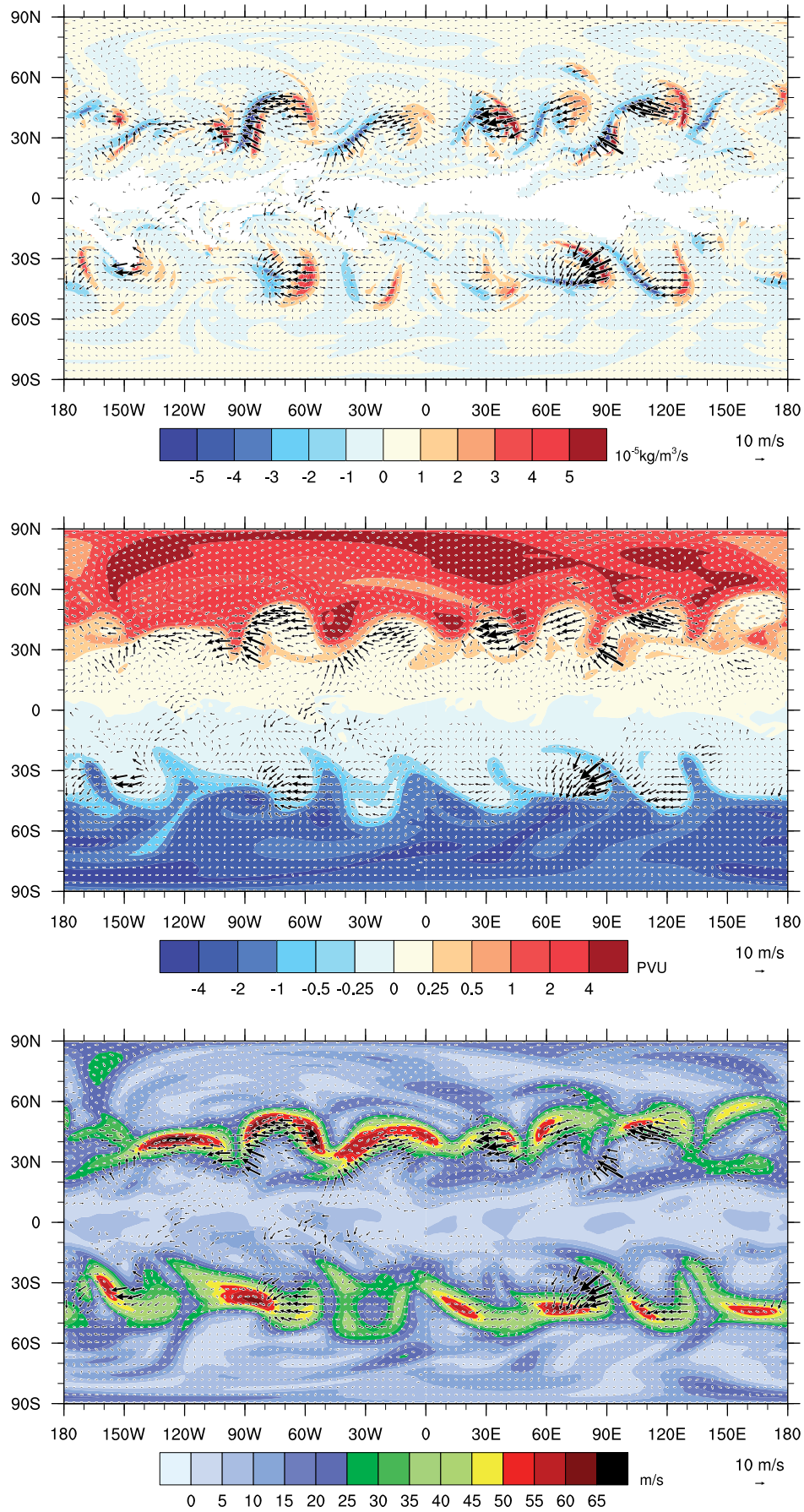

Figure 4: Active horizontal wind vectors in about 300 hPa. $\mathbf{v}_a$ is set undefined in the area near the equator where the EPV becomes insignificant. Color-shaded are DSI* (upper panel), P (middle panel), $|\mathbf{v}|$ (lower panel).

not transform kinetic energy into available energy regardless whether or not inactive flow is actually encountered. In a mean climate, the energy conversion process is in fact not reversible because all energy conversions are slightly nonlinear and contribute to the development of an energy cascade. If waves are breaking they feed energy into the small scale end of the cascade. The mass ends up with a smaller B-value after this cascading process. The ultimate friction generates frictional heating, a diabatic process which leads again to the crossing of isentropes.

Fig. 6 summarizes the mentioned processes. The zonal and time-mean meridional and vertical winds are not vanishing. Rather we see a dominating meridional flow in the upper troposphere at around 30 ° North. The black arrows symbolize a dominating flow that crosses the B-isolines indicating nonlinear wave-breaking in this region. Further to the North, but more in the mid-troposphere, we find a dominating downward movement and the arrows indicate a net crossing of θ-isolines. Wave-breaking and diabatic heating/cooling may occur partly simultaneously. The black arrows indicate only the locally dominating process.

It should be kept in mind that the active mass flux is divergent, both locally and when zonally averaged. The divergence of active mass flux is essential to attain information about that part of the inactive mass flux which detrains to the class of the net, or active, mass flux. The places where mass detrains from the inactive part and where mass entrains to the inactive part are not necessarily collocated in the meridional plane. Therefore we cannot expect that the net zonally averaged atmospheric active mass flux is non-divergent in the meridional plane, as it is actually seen in Fig. 6. This is similar to Lagrangian-mean flow which is generally divergent, too (Andrews et al., 1987, Section 3.7.1.).

We can also analyze the time mean three-dimensional field of the active wind. To illustrate this with the simple setting of the Held-Suarez test, the testcase was run with an elliptically shaped mountain range as explained in the introduction. This mountain range permanently triggers Rossby waves additionally to the already present baroclinic waves. Fig. 7 visualized the time mean horizontal active wind vectors at approximately 300 hPa in a region in the vicinity of the mountain range. Most of the active wind is in fact directed westward, that is against the prevailing eastward directed jet. As explained previously when discussing the wind speed pattern in Fig. 4 (lower panel), this indicates a permanent eastward movement of the waves. The typical Rossby wave pattern with southward bending of the mean flow immediately behind the mountain followed by a northward bending is reflected by the active wind pattern. The magnitude of the horizontal wind vector is enhanced by up to 30 % immediately behind the mountain range. This can be understood by the fact that the zonal phase speed of Rossby waves depends on the horizontal scale of the disturbances via

$$c_x = \bar{u} - \beta/K^2. \tag{2.25}$$

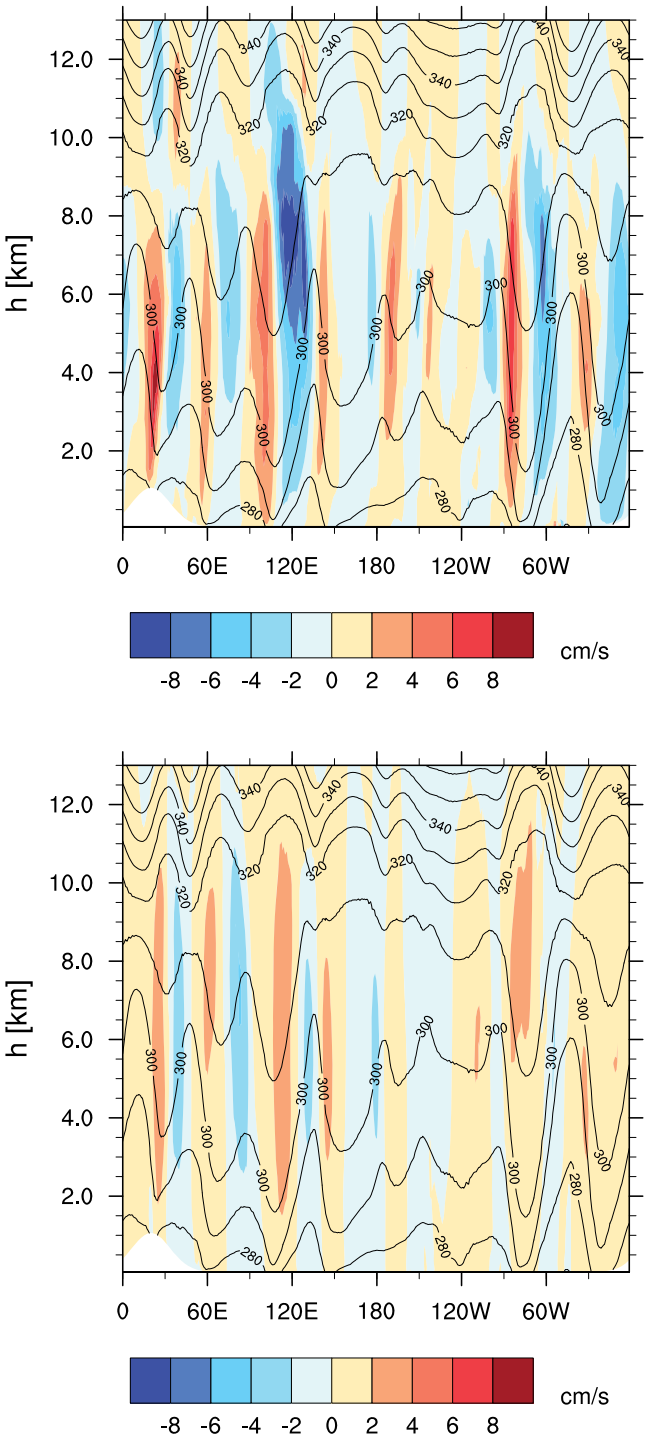

Figure 5: Active (upper) and actual (lower) vertical wind at 45 ° North together with θ-isolines.

Orographically undisturbed waves have a typical horizontal scale of 6000 km. The horizontal scale of the additionally excited waves due to the overflow over the mountain range is much smaller than this. Remember that the half-width of the mountain range is only 1500 km. The smaller scales enhance the speed of Rossby wave propagation. This is reflected by an increase of the magnitude of the active wind.

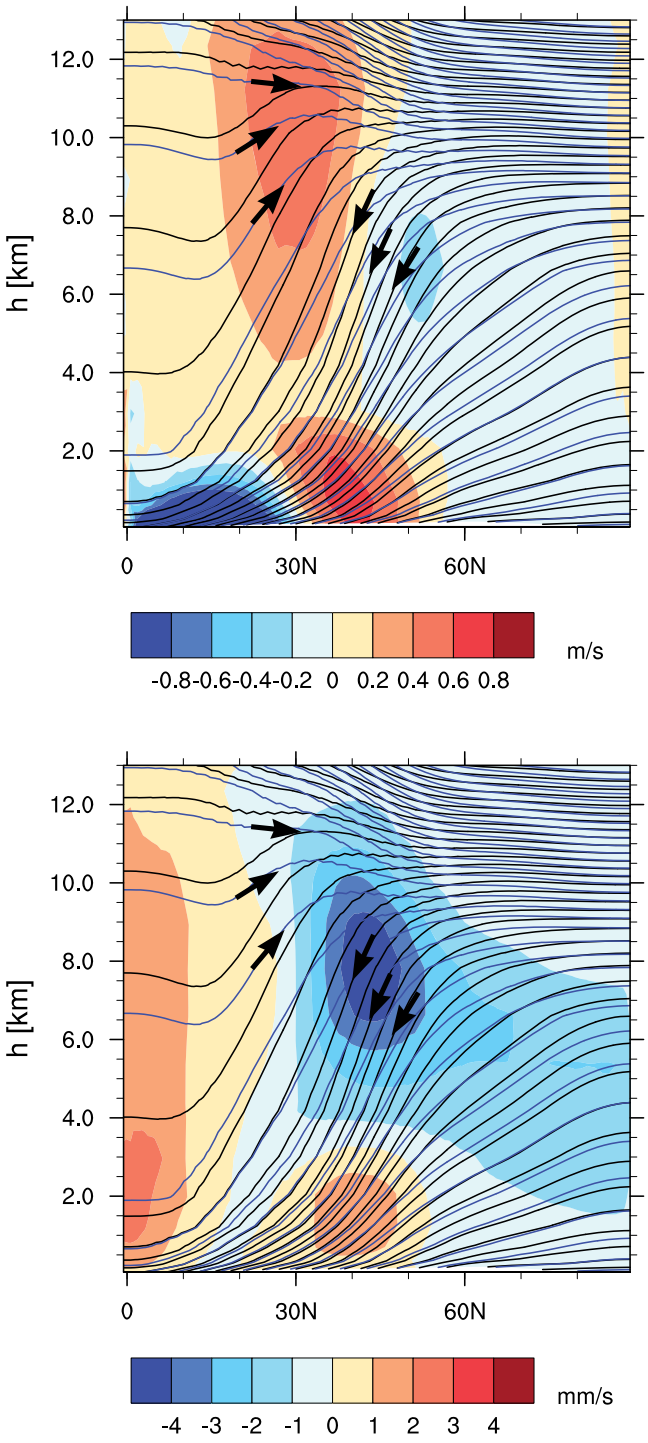

Figure 6: Zonal and time mean active meridional (upper panel) and vertical (lower panel) wind together with zonal and time mean θ-isolines (blue, increment 3 K) and B-isolines (black, increment 2000 J/kg). Arrows signify dominating processes that lead to the crossing of respective isolines.

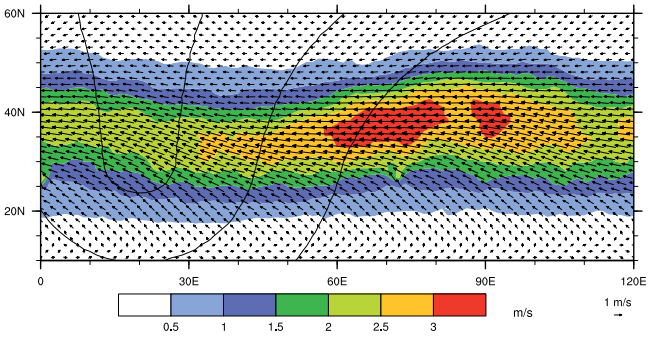

Figure 7: Time mean direction and magnitude of horizontal active wind at approximately 300 hPa in the vicinity of the mountain range (orography isolines for 1m, 100 m, and 800 m).

In Fig. 7 we also remark slightly enhanced active wind magnitudes and slightly differently directed vectors at some single points at around 26 ° North. These are the places where the pentagonal grid boxes of the ICON-IAP model are located. The icosahedral base structure of the underlying mesh leads there to a degradation of numerical accuracy of the numerical operators of the model as well as of those used for the active wind diagnosis. It is not clear which of those degraded operators leads to the observed dots. However, the further environment of the pentagon points seems not to be affected by the local degradation of numerical accuracy.

3 Comparison to wave-confined TEM viewpoint

The zonally averaged active wind and the residual wind share the property that they vanish if the flow is non-accelerated. However, the meaning of non-acceleration is different in both perspectives. The active wind vanishes for locally steady, frictionless and adiabatic flow, whereas the residual wind vanishes for steady, linear, frictionless, and adiabatic waves. Therefore the relation between the zonally averaged wind field of idealized waves $\{\bar{v}^{\mathrm{wave}}, \bar{w}^{\mathrm{wave}}\} = -\{v^{\mathrm{St}}, w^{\mathrm{St}}\}$ and the zonally averaged inactive flow $\{\bar{v}_{ia}, \bar{w}_{ia}\}$ is of interest here. Which approximations have to be done to the latter to arrive at the former? It will now be demonstrated that the zonally averaged inactive flow gives the negative Stokes drifts under the assumptions of linearity, dominance of hydrostatic and geostrophic balance, and quasi-uniform stratification. In detail, the assumption of linearity includes here that the kinetic energy $\mathbf{v}^2/2$ in the Bernoulli function is neglected and that absolute vorticity is dominated by the Earth vorticity. The assumptions of quasi-uniform stratification and the dominance of Earth vorticity are equivalent to the assumption of quasi-uniform ϱP.

For the mentioned comparison we start from

$$w_{ia} = \frac{\partial_x\theta(\partial_y B - c_p\Pi\partial_y\theta) - \partial_y\theta(\partial_x B - c_p\Pi\partial_x\theta)}{\boldsymbol{\omega}_a \cdot \nabla\theta}. \quad (3.1)$$

Assuming the dominance of the geostrophic winds and the fact that the geostrophic wind is non-divergent, one

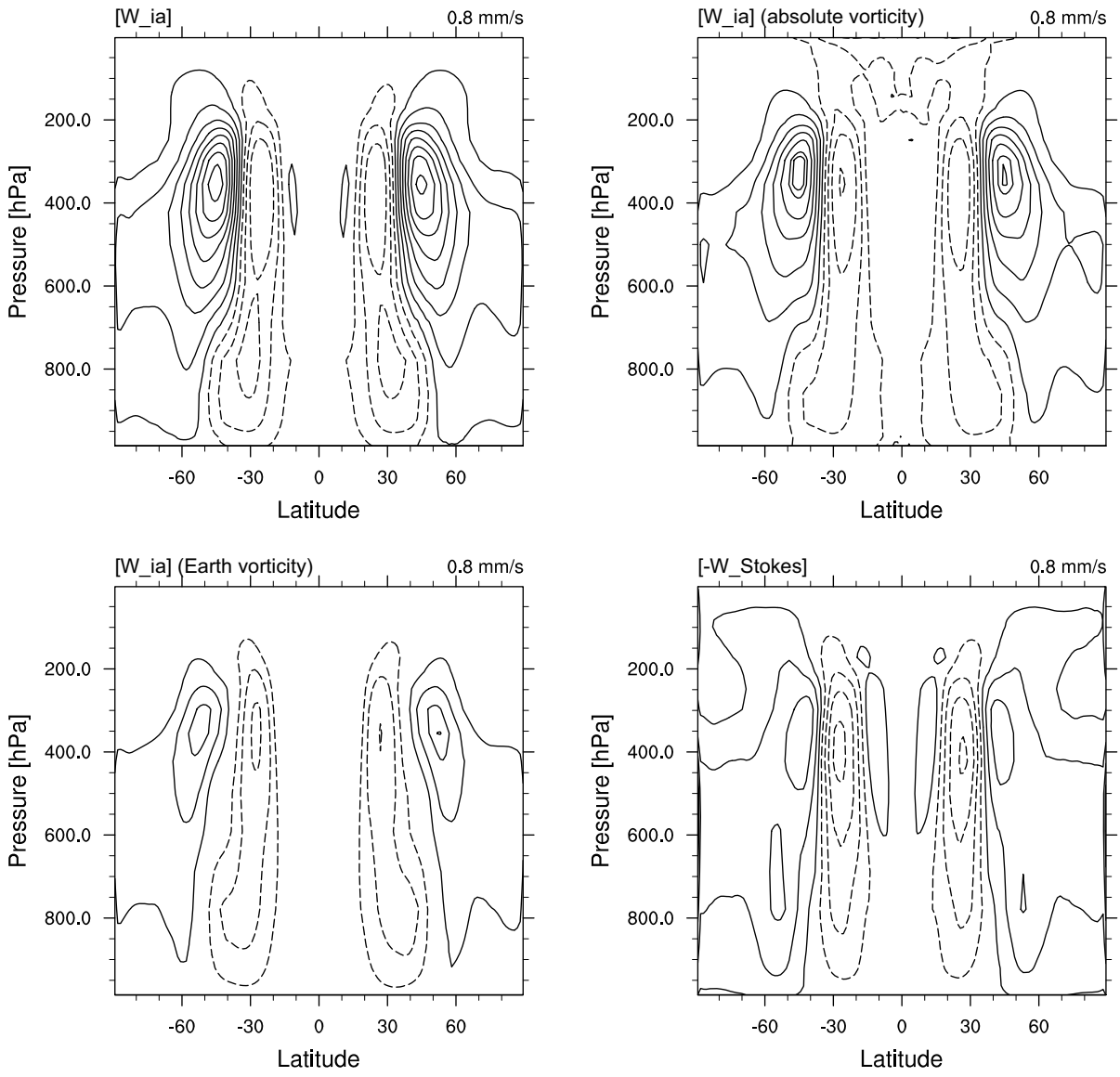

Figure 8: Visualization of approximation steps from $\overline{w_{ia}}$ to $-w^{\mathrm{St}}$ (see text).

obtains for the zonal average

$$\overline{w_{ia}} \approx \frac{\overline{-u_g\partial_x\theta - v_g\partial_y\theta}}{\overline{\partial_z\theta}} \approx \frac{\overline{-\partial_x(u_g\theta) + \theta\partial_x u_g - v_g\partial_y\theta}}{\overline{\partial_z\theta}}$$
$$\approx \frac{\overline{-\theta\partial_y v_g - v_g\partial_y\theta}}{\overline{\partial_z\theta}} \approx -\frac{1}{\varrho_r}\frac{\partial}{\partial y}\frac{\overline{\varrho_r v'\theta'}}{\overline{\partial_z\theta}} = -w^{\mathrm{St}}. \qquad (3.2)$$

The last step introduces a height dependent reference density and assumes quasi-uniform stratification. The vertical Stokes drift of zonally averaged idealized linear waves is expressed via a mass streamfunction $\psi = \overline{\varrho_r v'\theta'}/\overline{\partial_z\theta}$. Due to an imposed non-divergence constraint the meridional Stokes drift is

$$v^{\mathrm{St}} = -\frac{1}{\varrho_r}\frac{\partial}{\partial z}\frac{\overline{\varrho_r v'\theta'}}{\overline{\partial_z\theta}}. \qquad (3.3)$$

Different approximation steps from $\overline{w_{ia}}$ to $-w^{\mathrm{St}}$ for the Held-Suarez experiment elucidate the cause of the difference between these two (Fig. 8). The upper left panel shows the zonal mean inactive vertical velocity. Next, instead of the scalar product $\boldsymbol{\omega}_a \cdot \nabla\theta$ in the denominator, its simplified version $(\boldsymbol{\omega}_a \cdot \mathbf{k})\partial_z\theta$ is used (upper right panel). Those two panels are still rather similar. In the following step, the absolute vorticity has been replaced by the Coriolis parameter f (lower left panel). Compared to the previous panel, the main features are still visible, but the amplitude especially in the poleward half is significantly reduced. The lower right panel displays the negative Stokes drift, which is rather similar to the now previous panel. The sequence of figures demonstrates that the main approximation which leads to differences between $\overline{\mathbf{v}_{ia}}$ and $-\mathbf{v}^{\mathrm{St}}$ is the assumption that the denominator of (3.1) is a quasi-constant value. This allows us to put the denominator under a differential stemming from an expression in the numerator. By this procedure a stream function can be generated and the flow associated with idealized waves is forced to become non-divergent.

The assumption of the quasi-uniform denominator and hence a non-divergent Stokes drift leads to the *coincidence* of an averaged continuity equation for the TEM residual mass fluxes and the zonal mean part of the potential vorticity equation. This means for the meridional plane

$$\begin{aligned}
&\nabla\cdot(\overline{\varrho\mathbf{v}_a P-\boldsymbol{\omega}_a Q+\nabla\theta\times\mathbf{F}_r})\\
&=\nabla\cdot(\overline{\varrho}\widehat{\mathbf{v}_a}\widehat{P})+\nabla\cdot(\overline{\varrho\mathbf{v}_a P''-\boldsymbol{\omega}_a Q+\nabla\theta\times\mathbf{F}_r})\\
&\approx\frac{f\overline{\partial_z\theta}}{\varrho_r}\nabla\cdot(\varrho_r\mathbf{v}^*)+\nabla\cdot(\overline{\varrho\mathbf{v}_a P''-\boldsymbol{\omega}_a Q+\nabla\theta\times\mathbf{F}_r})\\
&\approx\nabla\cdot(\overline{\varrho\mathbf{v}_a P''-\boldsymbol{\omega}_a Q+\nabla\theta\times\mathbf{F}_r}). \qquad (3.4)
\end{aligned}$$

We can loosely interpret the eddy flux term $\overline{\varrho\mathbf{v}_a P''}$ as the representative of the Eliassen-Palm flux divergence known from the quasi-geostrophic limit. Its vertical component is then neglected. In climatological steady state, the last line of (3.4) vanishes. This is one of the central facts in the TEM framework as mentioned in Andrews et al. (1987) (Section 7.2.1, Equation 7.2.4c). It says that the eddy forcing and the diabatic heating/cooling are linked in a closed circulation.

We have thus identified the enforced non-divergent residual mass flux as the central point that distinguishes the wave-confined TEM viewpoint from the flow-confined active wind viewpoint.

In steady state, it is not the divergence of the active mass flux which vanishes, but the total flux of EPV. For such a steady state, we can write[3]

$$\begin{aligned}
&\overline{\varrho}\widehat{\mathbf{v}_a}\widehat{P}+\overline{\varrho\mathbf{v}_a'' P''}-\overline{\boldsymbol{\omega}_a Q}+\overline{\nabla\theta\times\mathbf{F}_r}\\
&=\overline{\nabla\theta\times\partial_t\mathbf{v}-\boldsymbol{\omega}_a\partial_t\theta}\quad(=0). \qquad (3.5)
\end{aligned}$$

The expression (3.5) is a vector equation and has similarities to both, the TEM horizontal momentum and temperature equations. One difference is that the eddy flux term occurs here not as a part of the transformed zonal momentum equation, but as a term which is linked to both, the thermal and the dynamical part of the comparable TEM equation set. As a consequence, eddy EPV-fluxes will not only represent the horizontal part of a secondary circulation, but also contribute to its vertical part. The thermal wind relation as a component of the TEM equation set is not needed here, because it is in fact a steady state version of the meridional momentum equation. A transformed version of the meridional momentum equation is included in (3.5).

Let us now compare the zonally averaged residual and active mass fluxes for the Held-Suarez test. The TEM diagnostics which is used for a comparison with the active wind diagnostics employs the difference stream function ψ_1 of Hardiman et al. (2010). All zonal averages are calculated on model levels, but for the figures, the diagnosis is displayed in a pressure coordinate system. All values of the active wind are set undefined if the absolute EPV-value drops below one thousandth of the maximum absolute EPV-value in the considered model level.

Fig. 9 displays three types of zonally averaged vertical and meridional winds. The three types are obtained from the conventional Eulerian mean $(\widehat{v}_{\mathrm{Eul}}, \widehat{w}_{\mathrm{Eul}})$, the TEM residual mean (v^*, w^*), and the active mean $(\widehat{v}_a, \widehat{w}_a)$. Since the mountain range is only inserted on the northern hemisphere, the pattern of all mentioned wind components are not symmetric about the equator. The conventional Eulerian mean circulation reflects the well-known three-cell structure of the hemispheric circulation, which consists of the Hadley, Ferrel, and polar cells. The TEM residual and the active means reveal relatively similar structures in the upper troposphere, but very different behavior in the boundary layer. As expected from the TEM residual winds, we recognize a direct overturning cell with rising motion in the tropics, a poleward motion in mid-latitudes, sinking air in polar latitudes and a near-surface return flow towards tropical latitudes. The active wind zonal average is also characterized by tropical upwelling. The mean vertical downward active wind in the mid-latitude's free troposphere is much stronger than in the TEM residual case whereas the the mean meridional wind is a bit weaker. The upward and poleward bending branch of active winds is clearly visible. The return flow towards the tropics is very different from the TEM case: There is a poleward and upward motion in mid-latitudes in the boundary layer. The active meridional wind is comparable to the Eulerian mean meridional wind in this region. This is not true for the vertical wind. Therefore the Eulerian mean and the active wind vector mean is quite distinct even in the boundary layer.

How can this, at first glance unexpected, pattern of the active wind components be interpreted? For this purpose the different terms of (3.5) are investigated in their vertical and meridional components. A rough estimate of those terms yields

$$\hat{v}_a\approx-\frac{\overline{\varrho v_a'' P''}}{\bar{\varrho}\hat{P}}+\frac{\overline{Q}\,\overline{\partial_z u}}{\overline{\omega_{z,a}}\,\overline{\partial_z\theta}}+\frac{\overline{k_v}\,\overline{u}}{\overline{\omega_{z,a}}\,\overline{\partial_z\theta}} \qquad (3.6)$$

$$\hat{w}_a\approx-\frac{\overline{\varrho w_a'' P''}}{\bar{\varrho}\hat{P}}+\frac{\overline{Q}}{\overline{\partial_z\theta}}-\frac{\overline{k_v}\,\overline{u}\,\overline{\partial_y\theta}}{\overline{\omega_{z,a}}\,\overline{\partial_z\theta}}. \qquad (3.7)$$

Here, Q and k_v are the heating function and the Rayleigh friction coefficient of the Held-Suarez testcase. Note that the Rayleigh friction suggested in the testcase is physically questionable as it is not given as a divergence of a stress tensor. The horizontal momentum diffusion of the ICON-IAP model is omitted in the diagnosis. The covariances of the heating and friction terms are also omitted. Because of these approximations we cannot expect that the sum of the three terms in (3.6) and (3.7) represents exactly the active wind distributions of Fig. 9. We refer to the three terms as active EPV eddy transport term, heating term, and friction term, respectively.

[3]The hat-average means a mass-weighted mean (Hesselberg mean) in contrast to the more common Reynolds mean. The double primes signify deviations from this mass-weighted mean.

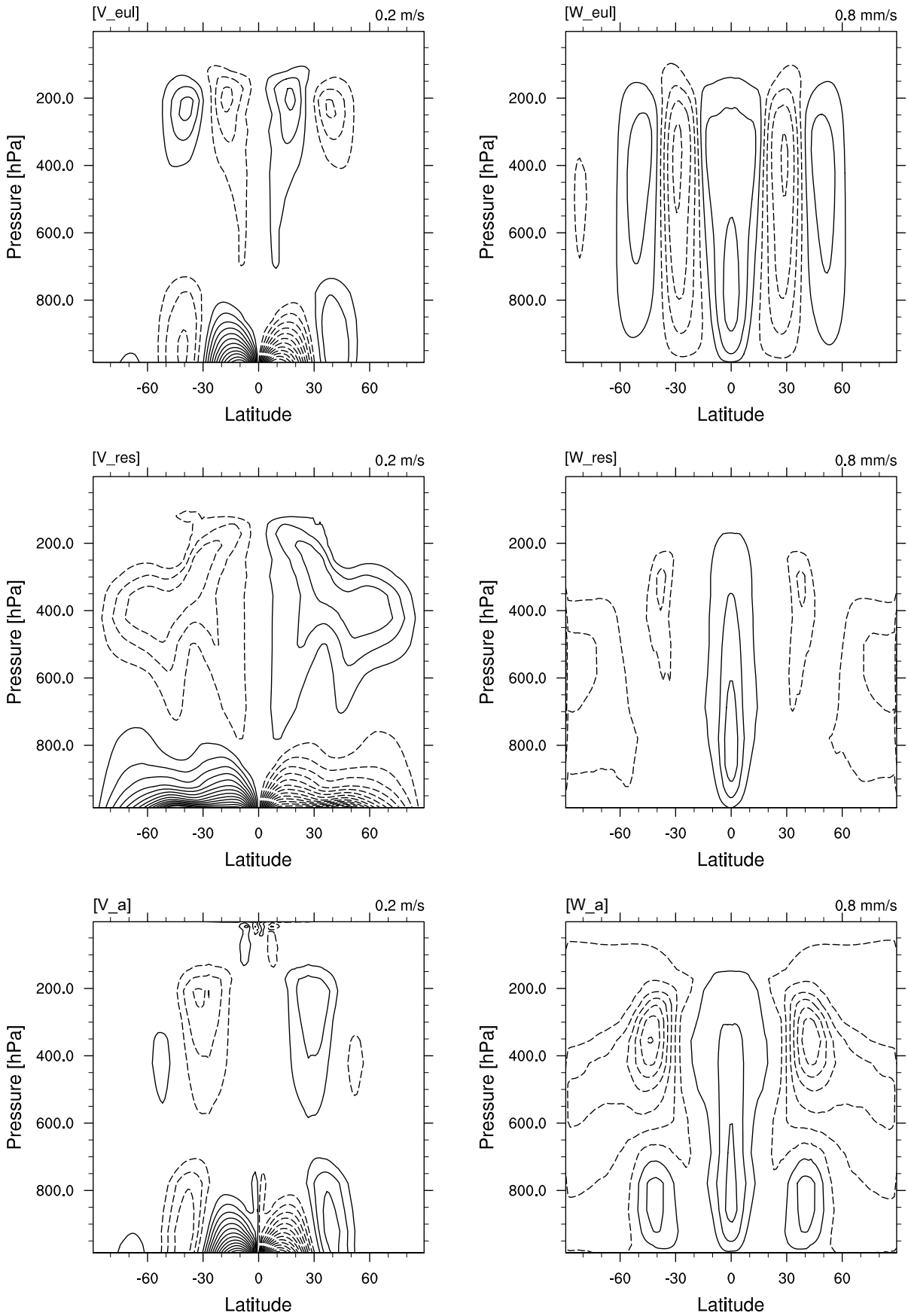

Figure 9: Zonal means of meridional (left column, contour intervals 0.2 m/s) and vertical (right column, contour intervals 0.8 mm/s) winds. First row: conventional Eulerian mean. Second row: TEM residual mean. Third row: active wind mean.

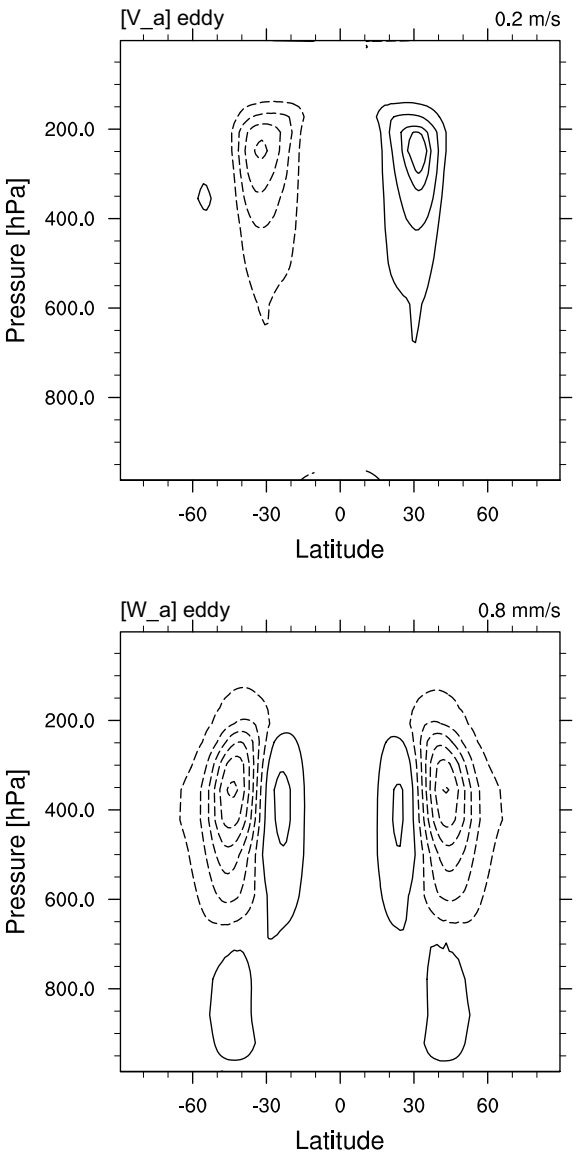

Figure 10: Meridional (upper panel) and vertical (lower panel) active EPV-flux term contributions to the zonally averaged active winds. The contour intervals are chosen such as to conform with those of Fig. 9. Values ±10 ° around the equator are not shown.

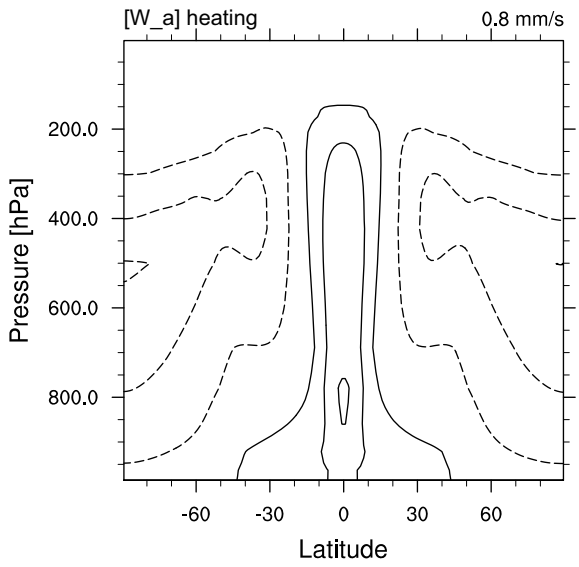

Figure 11: Heating term contribution to the zonally averaged vertical active wind. The contour interval is chosen such as to conform with that of the right column of Fig. 9.

Fig. 10 displays the active meridional and vertical eddy transport terms of EPV. We see that those eddy EPV-fluxes explain roughly the mean active winds in the upper troposphere and also partly the rising motion in the mid-latitudes boundary layer. The meridional active eddy EPV-flux term is in very good balance with the mean active meridional wind in the upper troposphere. The locations of the meridional active eddy EPV-fluxes are to be found in approximately 300 hPa at around 30 ° from the equator. These are roughly the same positions where also the TEM meridional winds exhibit parts of their maxima. The more poleward pattern of v^* are, however, not reproduced by $\widehat{v}_a$. The reason is evident from the comparison of the upper left and lower right panel of Fig. 8. The largest differences between w_{ia} and $-w^{\mathrm{St}}$ are poleward of about ±40 °. A smaller amplitude of $-w^{\mathrm{St}}$ in comparison to w_{ia} does not let the residual flow bend downward quickly enough. This enhances the possibility for v^* to reach higher latitudes. The vertical active eddy EPV-flux term is quite strong in the upper troposphere. This eddy flux term contributes to an overall stronger $\widehat{w}_a$ compared to w^*. The TEM framework does not provide a place for the inclusion of the vertical eddy flux term of EPV.

Fig. 11 displays the heating term that occurs in the equation for the mean vertical active wind. We see that this term balances the polar sinking and the equatorial rising of air. Its pattern resembles roughly both, $\widehat{w}_a$ and w^*. Hence, the familiar vertical motion picture obtained with the TEM equations is approximately recovered. The heating term does not yield any notable contribution onto $\widehat{v}_a$ (not shown).

Last, we inspect the friction terms (Fig. 12). The equatorial convergence in the active meridional wind is associated with friction. Additionally we encounter a mid-latitude poleward flow, which is not present in the v^* equatorward return flow. The upward motion in mid-latitudes' boundary layer is also mainly attributable to friction. The pattern of both, meridional and vertical, active winds can be explained by dominating mid-latitude low pressure around 55 ° and subtropic high pressure a bit poleward of 30 °. Frictionally induced inflow occurs for the lows and the reverse is to be found for the highs, as known from the Ekman layer dynamics and made visible in Fig. 3. This kind of plausible frictional flow is not seen in the plots for the TEM residual winds.

Summarizing, we obtain a qualitatively convincing explanation about the different contributions that balance the active vertical and meridional winds. However, unlike the TEM residual winds, the active winds do not exhibit a closed circulation. This is already eye-catching in the $\widehat{v}_a$-plot in Fig. 9. We observe a net poleward active

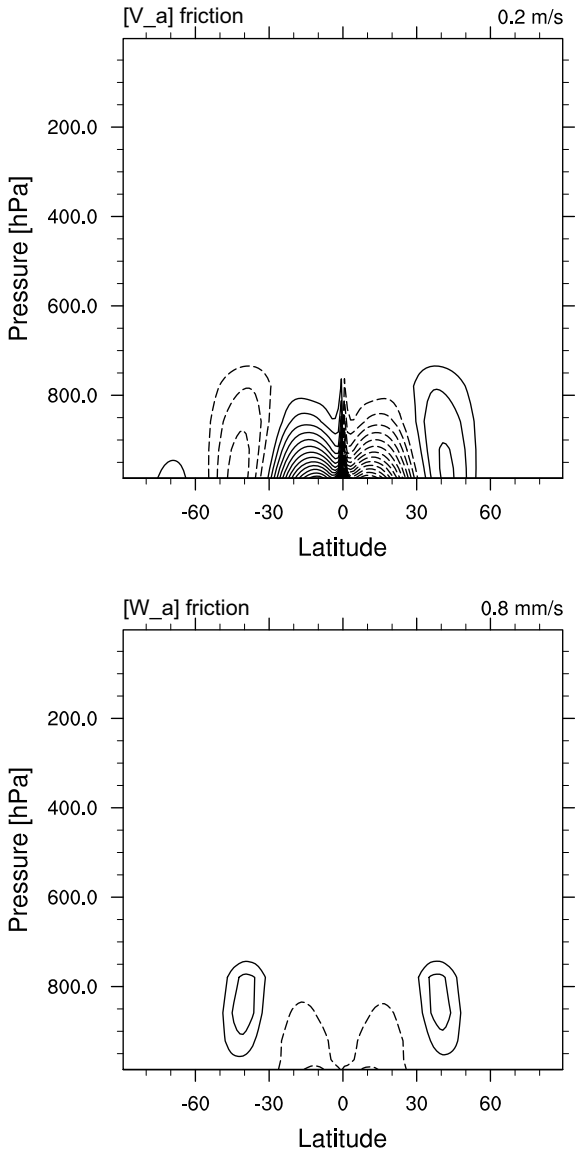

Figure 12: Friction terms that contribute to balance the zonally averaged meridional (upper panel) and vertical (lower panel) active winds. The contour intervals are chosen such as to conform with those of Fig. 9.

wind at all heights around 35 ° latitude. The active wind displays the mass fluxes that are outside the $\nabla\theta \times \nabla B$ tubes. The place where mass fluxes are forced out of their inactive orbits and back into inactive orbits can be everywhere, in particular not necessarily in the same altitude and latitude. The inactive mass flux can also transport mass, but without net effects on atmospheric mass distribution. Only the total mass flux is non-divergent in the time mean.

4 Conclusion

In this paper, a local version of the transformed Eulerian (but not: mean) equations, namely equations (2.12) and (2.13), was derived. The most important point was to recognize that the transformed velocities $\mathbf{v}_a$ are in fact deviations from the inactive wind $\mathbf{v}_{ia}$ associated with a local energy-vorticity equilibrium state. The inactive flow part $\mathbf{v}_{ia}$ is dynamically dead. It does neither participate in kinetic energy conversions nor does its EPV-flux has any effect. Therefore, it cannot contribute to an acceleration of the local flow and so do neither for a mean flow. The inactive wind can be seen as a generalization of the geostrophic wind under consideration of inertial forces and the constraint of adiabatism.

The question of non-acceleration of a mean flow was a long-standing question of dynamicists, and was answered historically with the concept of a vanishing Eliassen-Palm flux divergence under non-acceleration conditions. However, the TEM framework needed the idealization of propagating linear waves on a basic zonal flow.

What can be learned from the new perspective? We can definitely not explain more about the residual circulation than what was possible with the TEM framework, especially not if we appreciate recent developments towards 3-dimensional TEM equations (Kinoshita et al., 2010). We can even less explain, because the downward-control principle (Haynes et al., 1991) does not work. The downward-control principle works because the residual circulation is non-divergent. The new theory explained in the paper is not non-divergent in the meridional plane. It shares this property with Lagrangian-mean flow.

Several findings are worth to be highlighted. First, the local picture of $\mathbf{v}_a$ already points to the fact that the filamentation of vorticity as an indicator of breaking Rossby waves is associated with a poleward mass flux. Second, the transport barrier property of a steep EPV gradient is obvious to the naked eye. Third, the new formulation allows a much more credible representation of boundary layer flow. Ekman dynamics is now represented in the zonal mean picture. Fourth, the Bernoulli function was identified as the isosurface to be crossed during wave breaking. Fifth, the DSI* turned out to act as a source for the divergence of the active mass flux.

There are some striking features that are perhaps important for the further working with residual flows. Whereas in the upper troposphere in low latitudes the meridional winds are quite similar for the residual and the zonal-mean active viewpoints, the flow poleward of about 40 ° latitude is quite different. Therefore, some care has to be taken when interpreting residual winds.

The active wind is not only a concept applicable in the context of large-scale dynamics. The EPV is not always dominated by the vertical component of vorticity. Rather it can become dominated by horizontal components of vorticity which are associated with strong vertical wind shear. This is the case for smaller scale gravity waves. Hence, the concept of active winds opens a possibility for a detailed study of the contribution of breaking gravity waves to net mass fluxes especially in the mesosphere.

References

Andrews, D.G., M.E. McIntyre, 1976: Planetary waves in horizontal and vertical shear: The generalized Eliassen-Palm relation and the mean zonal acceleration. – J. Atmos. Sci. **33**, 2031–2048.

Andrews, D.G., M.E. McIntyre, 1978: Generalized Eliassen-Palm and Charney-drazin theorems for waves on axisymmetric mean flows in compressible atmospheres. – J. Atmos. Sci. **35**, 175–185.

Andrews, D.G., J.R. Holton, C.B. Leovy, 1987: Middle atmosphere dynamics – Academic Press, San Diego, 500 p.

Boyd, J.P., 1976: The noninteraction of waves with the zonally averaged flow on a spherical Earth and the interrelationships of eddy fluxes of energy, heat and momentum. – J. Atmos. Sci. **33**, 2285–2291.

Claussnitzer, A., P. Névir, I. Langer, E. Reimer, U. Cubasch, 2008: Scale-dependent analyses of precipitation forecasts and cloud properties using the Dynamic State Index. – Meteorol. Z. **17**, 813–825.

Davies-Jones, R., 2003: Comments on "A generalization of Bernoulli's theorem". – J. Atmos. Sci. **60**, 2039–2041.

Gassmann, A., 2013: A global hexagonal C-grid non-hydrostatic dynamical core (ICON-IAP) designed for energetic consistency. – Quart. J. Roy. Meteor. Soc. **139**, 152–175.

Hardiman, S., D.G. Andrews, A.A. White, N. Butchart, I. Edmond, 2010: Using different formulations of the transformed Eulerian mean equations and Eliassen-Palm diagnostics in general ciruclation models. – J. Atmos. Sci. **67**, 1983–1995.

Haynes, P.H., M.E. McIntyre, 1987: On the evolution of vorticity and potential vorticity in the presence of diabatic heating and frictional or other forces. – J. Atmos. Sci. **44**, 828–841.

Haynes, P.H., M.E. McIntyre, 1990: On the conservation and impermeability theorems for potential vorticity. – J. Atmos. Sci. **47**, 2021–2031.

Haynes, P.H., H.J. Marks, M.E. McIntyre, T.G. Shepherd, K.P. Shine, 1991: On the "downward control" of extratropical diabatic circulations by eddy-induced mean zonal forces. – J. Atmos. Sci. **48**, 651–678.

Held, I.M., M.J. Suarez, 1994: A proposal for the comparison of the dynamical cores of atmospheric general circulation models. – Bull. Amer. Meteor. Soc. **75**, 1825–1830.

Holton, J.R., 2004: An introduction to dynamic meteorology, Fourth Edition – Elsevier Academic Press, New York, London, 535 p.

Kinoshita, T., Y. Tomikawa, K. Sato, 2010: On the three-dimensional residual mean circulation and wave activity flux of the primitive equations. – J. Meteor. Soc. Japan **88**, 373–394.

Lange, H.-J., 2002: Die Physik des Wetters und des Klimas. Ein Grundkurs zur Theorie des Systems Atmosphäre. – Dietrich Reimer Verlag Berlin, 625 S.

McIntyre, M.E., W.A. Norton, 1990: Dissipative wave-mean interactions and the transport of vorticity or potential vorticity. – J. Fluid. Mech. **212**, 403–435.

Plumb, R.A., R. Ferrari, 2005: Transformed Eulerian-mean theory. part I: Nonquasigeostrophic theory for eddies on a zonal-mean flow. – J. Phys. Oceanogr. **35**, 165–174.

Schär, C., 1993: A generalization fo Bernoulli's theorem. – J. Atmos. Sci. **50**, 1437–1443.

Vallis, G.K., 2006: Atmospheric and oceanic fluid dynamics – Cambridge University Press, Cambridge, 745 p.

Weber, T., P. Névir, 2008: Storm tracks and cyclone development using the theoretical concept of the Dynamic State Iindex DSI. – Tellus **60A**, 1–10.